

A possible gravitational lens in the Hubble Deep Field South¹

Rennan Barkana², Roger Blandford, David W. Hogg³

Institute for Advanced Study, Olden Lane, Princeton, NJ 08540, USA

ABSTRACT

We model an apparent gravitational lens system HDFS 2232509–603243 in the Hubble Deep Field South. The system consists of a blue $V = 25$ mag arc separated by $0''.9$ from a red $V = 22$ mag elliptical galaxy. A mass distribution which follows the observed light distribution with a constant mass-to-light ratio can fit the arc component positions if external shear is added. A good fit is also obtained with simple parameterized models, and all the models predict a fourth image fainter than the detection limit. The inferred mass-to-light ratio is ~ 15 in solar units if the lens is at $z = 0.6$. Prospects for obtaining spectroscopic redshifts of the elliptical galaxy and the arc are good.

Subject headings: galaxies: individual: HDFS 2232509–603243 — gravitational lensing — cosmology

1. Introduction

Detailed studies of gravitational lenses have provided a wealth of information on galaxies (e.g., Schneider, Ehlers, & Falco 1992; Blandford & Narayan 1992). In each lensed system, the mass distribution of the lens galaxy is directly constrained by its bending of light, while the lens provides a natural telescope through which the source can be observed and studied. The statistical properties of multiply imaged sources can provide additional information on the typical mass distribution in galaxies and on the cosmological world model (e.g., Turner, Ostriker, & Gott 1984, Kochanek 1996).

The extraordinary resolution of the Hubble Space Telescope (HST) has allowed for the first time the detection of lenses where both the source and the deflector are “normal” optically-selected galaxies, with sub-arcsecond image separations, which are very difficult to detect from the ground. Ratnatunga et al. (1995) discovered two examples of four-image “Einstein cross” gravitational

¹Based on observations made with the NASA/ESA Hubble Space Telescope, which is operated by AURA under NASA contract NAS 5-26555

²email: barkana@ias.edu

³Hubble Fellow

lenses in the Groth-Westphal strip. They found that they could model these lenses with mass distributions elongated in the same direction as the observed lens galaxies except for a rotation of about 10° . The mass models, however, required ellipticities substantially above those of the light distributions, suggesting (as is commonly suspected in radio lenses) that some external shear is important to the lensing.

The Hubble Deep Field (HDF, Williams et al. 1996), the deepest set of exposures taken with the HST, has enabled an unprecedented study of galaxy morphological evolution (e.g., Ellis 1998) and the global star formation history (e.g., Madau, Pozzetti, & Dickinson 1998). Candidate gravitational lenses were reported by Hogg et al. (1996), who noted on the basis of radio surveys that several lenses are expected in the HDF. However, after further observations not one strong case for multiple imaging has been identified (Zepf, Moustakas, & Davis 1997, Cohen 1998). This shortage of lenses may provide a challenge for some cosmological models (Cooray, Quashnock, & Miller 1998).

The Southern Hubble Deep Field (HDF-S, Williams et al. 1998) is a second set of ultra-deep HST exposures, providing an opportunity for discovering more lenses and for roughly doubling the power of lens statistics by combining the two HDF fields. The best candidate lens, noted by the HDF-S team (Williams 1998), consists of a blue arc about $0''.9$ from an elliptical galaxy. The arc is resolved tangentially into three images with the two brighter ones almost merged together, a typical image configuration if the source is near a cusp. The arc extends only a few pixels in the radial direction. In this *Letter* we report on a more detailed study of this arc and argue that it is a bona fide multiply imaged source.

We assume a world model of $\Omega = 0.3$ in matter and no cosmological constant, unless otherwise specified. We also set $H_0 = 100 h \text{ km s}^{-1} \text{ Mpc}^{-1}$.

2. Observations

The WFPC2 HDF-S is a $\sim 5 \text{ arcmin}^2$ field centered on $22\ 32\ 56.22 - 60\ 33\ 02.69$ (J2000), imaged with the WFPC2 instrument on the HST in the F300W, F450W, F606W, and F814W bandpasses for total exposure times of 1.4×10^5 , 1.0×10^5 , 8×10^4 , and 1.0×10^5 s respectively, reaching point-source sensitivities of roughly $V = 29$ mag (Williams et al. 1998). The “version-1.0” reductions of the images clearly show a bright candidate lens system at pixel location $(2982.7, 2837.6)$ or $22\ 32\ 50.90 - 60\ 32\ 43.0$ (J2000). This candidate lens system will be called “HDFS 2232509–603243” hereafter.

The morphology of HDFS 2232509–603243 is that of a roughly $V = 22$ mag elliptical galaxy (hereafter “the elliptical”) with a much bluer multi-component arc (hereafter “the arc”) separated from the center of the elliptical by $0''.9$, in the direction -50° (north through east), as shown in Figure 1. There is also a faint point-like source (hereafter “the dot”) separated from the center of the elliptical by $0''.96$, in the direction $+53^\circ$.

The elliptical is very smooth and symmetrical, so images created by rotating the version-1.0 images through 180° (centered on the pixel nearest the center of the elliptical) and subtracting them from their unrotated originals show essentially no sign of the elliptical, at least at the angular radius of the arc. Photometry of the arc was performed in these “rotated-subtracted” images, through apertures which are partial annuli centered on the elliptical. The total F606W flux was measured through a partial annulus of inner radius $0''.517$ and outer radius $1''.194$, extending over position angles 0° through -108° . Colors were measured through a partial annulus of inner and outer radii $0''.677$ and $1''.035$, over -18° through -90° . These magnitudes are given in Table 1. Signal-to-noise ratios for the photometric measurements are also given. Because the version-1.0 reduction technique correlates nearby pixel values, the per-pixel rms noise levels used for computing signal-to-noise ratios were found by re-binning the image into pixels 4×4 times larger than the version 1.0 pixels. The rms was measured in these re-binned images and then scaled to the equivalent per-pixel value.

The arc appears to separate into four distinct components, labeled A, B, C and D, going clockwise around the arc. All four components have very similar colors. Components A, B, and D appear to have point-like centers with fuzz, while component C is more extended. Gaussians with the same FWHM as the seeing (4 pixels) were fit to components A, B and D, and a gaussian of variable width was fit to component C, all in the F450W rotated-subtracted image. The best-fit positions and fluxes of these gaussians are given in Table 2. We estimate position errors of a half pixel from fitting an artificial image.

The flux and colors of the dot were measured through a $0''.159$ radius circular aperture. These magnitudes are given in Table 1.

In order to make arc-free images of the elliptical, the region of each version 1.0 image in the partial annulus centered on the elliptical with inner and outer radii of $0''.517$ and $1''.194$, over position angles 0° through -108° were replaced with the corresponding regions diametrically opposite (i.e., at position angles rotated by 180°). These “arc-removed” images show virtually no evidence of the arc. The total F814W flux of the elliptical was measured out to its $2\text{-}\sigma$ (per pixel) isophote. The colors were measured through $0''.915$ radius circular apertures. These magnitudes are given in Table 1.

A de Vaucouleurs profile was fit to the radial profile of the elliptical in the “arc-removed” images. The effective radius is $r_e = 0''.37$ and F814W-band surface brightness at the effective radius is 21.6 mag in each arcsec². The isophote ellipticity orientation varies with radius. The outer isophotes (radii $> 0''.8$) of the elliptical have ellipticity ~ 0.2 and are elongated along $+40^\circ$. The inner isophotes (radii $< 0''.3$) also have ellipticity ~ 0.2 but are elongated along -40° , i.e., almost orthogonal. Isophotes intermediate to these two regimes are fairly circular.

Comparison of the colors of the elliptical with HDF galaxies with known redshifts suggests that its redshift is roughly $z = 0.56$. This suggests a total luminosity of $8.7 \times 10^9 h^{-2} L_\odot$, or roughly L^* . This luminosity in the rest-frame B-band is obtained by interpolating between the observed

bandpasses. The luminosity is a factor of 3 larger if $z_L = 0.8$, and a factor of 6.5 smaller if $z_L = 0.3$.

3. Lens models

We consider several models for the lensing mass distribution, simple parameterized models as well as a constant mass-to-light ratio model. Since the arc is tangential the image positions are not very sensitive to the radial profile of the lens, so for the parameterized models we take it to be singular and isothermal. An axisymmetric mass distribution cannot produce a tangential arc (except for a full Einstein ring), so we consider two types of asymmetry. The first is external shear (with an axisymmetric galaxy), and the second is an elliptical galaxy (with no external shear). We assume that the arc components A, B and D are three images of a common source. Component C can easily be produced if the source is extended or multi-component. We do not include as constraints component C or the observed flux ratios among components A, B and D, since these are sensitive to the detailed flux distribution of the source. The dot is much fainter than the arc and may be an unrelated background source which is being magnified.

We consider a lens at redshift z_L and a source at z_S , with corresponding angular diameter distances to the observer D_L and D_S , and a lens-source distance D_{LS} . Then the two-dimensional potential ψ is determined by (e.g., Schneider et al. 1992; Blandford & Narayan 1992)

$$\nabla^2\psi = 2\frac{\Sigma}{\Sigma_c} \equiv 2\kappa, \quad (1)$$

where Σ is the projected mass density of the lens and the critical density is $\Sigma_c = c^2 D_S / (4\pi G D_L D_{LS})$.

The singular isothermal sphere (SIS) is defined by $\psi = br$ and a corresponding $\kappa = b/(2r)$. The parameter b is related to the velocity dispersion σ by

$$b = 4\pi \left(\frac{\sigma}{c}\right)^2 \frac{D_{LS}}{D_S}. \quad (2)$$

External shear is defined by adding to the potential the term

$$\psi_\gamma = -\frac{\gamma}{2}r^2 \cos 2(\theta - \theta_\gamma), \quad (3)$$

where γ is the shear strength and θ_γ is its direction. With this sign convention, if the shear were due to an axisymmetric galaxy then this galaxy would be located at an angle θ_γ from the lens galaxy. We measure all angles from North through East. We denote by SIS+ γ the SIS model with external shear.

The singular isothermal elliptical mass distribution (SIEMD) is given by $\kappa = b/[2(1 - \epsilon)r_\epsilon]$, where if the major axis is along the y -axis then

$$r_\epsilon^2 = \frac{y^2}{(1 + \epsilon)^2} + \frac{x^2}{(1 - \epsilon)^2}. \quad (4)$$

More generally we rotate the major axis by an angle θ_ϵ . The axis ratio is $a = (1 - \epsilon)/(1 + \epsilon)$. The lensing properties of the SIEMD have been studied analytically by Kassiola & Kovner (1993) and by Kormann, Schneider, & Bartelmann (1994).

We fit these two lens models, the SIS+ γ model and the SIEMD, to the three observed image positions, with results shown in Table 3. Both models have a single degree of freedom (dof). When determining parameter uncertainties we scale the errors so that a 1σ uncertainty is given by $\Delta\chi^2 = \bar{\chi}^2$.

Both lens models have an elongated diamond caustic, with the arc produced by a source near one of the four cusps. The cusp may be either on the major axis or the minor axis of the caustic, and the two possibilities produce different image configurations. We indicate a major cusp by [maj] and a minor cusp by [min]. Since the observed position B is farther from the center of the lens than A or D , the arc is more naturally produced by a minor cusp in which the middle image of the three is outside the critical curve while the outer two images are inside it. Indeed, in all the models the minor cusp is favored.

The SIEMD[min] model fits slightly better than the SIEMD[maj] model. In both models the ellipticity is not well determined, but the direction θ_ϵ is well determined. Interestingly, the orientation of the SIEMD[min] model agrees with the observed orientation of the outer isophotes of the galaxy, while the orientation of the SIEMD[maj] model is nearly orthogonal and agrees with the observed orientation of the inner isophotes. The SIS+ γ [maj] model produces a comparable fit to the SIEMD models, with a small shear, and an orientation in agreement with that of the SIEMD[maj] model. However, among the simple parameterized models only the SIS+ γ [min] model fits the data well (see Figure 2), while the others formally give a poor fit. The model requires a substantial shear ($\gamma = 0.26$) produced by objects lying in the NE or SW directions. To compute the mass-to-light ratio for various models, we fix a circle about the galaxy center of radius $0''.915$, which is the distance of component B. The luminosity of the galaxy within this circle is $7.6 \times 10^9 h^{-2} L_\odot$ if $z_L = 0.56$. If, e.g., $z_S = 1.5$, then $\Sigma_c = 0.895 \text{ g cm}^{-2}$ and the mass within the same circle of the SIS is $M = 2.1 \times 10^{11} h^{-1} (b/1'') M_\odot$. This yields a mass-to-light ratio of $27 h (b/1'')$, and a velocity dispersion $\sigma = 270 \sqrt{b/1''} \text{ km s}^{-1}$. Note that for the lenses which they considered, Keeton, Kochanek, & Seljak (1997) found a substantial improvement in the fits with a model which includes ellipticity as well as external shear, but the data on HDF5 2232509–603243 cannot yet constrain such a complex lens model.

As a second approach to modeling, we utilize the resolved image of the lens galaxy to construct a model with a constant mass-to-light ratio (labeled M/L in Table 3). After smoothing the light distribution with a 4-pixel FWHM Gaussian, we use Fourier methods to solve equation (1) for the potential. The pure M/L model has the mass-to-light ratio as its only parameter, and cannot fit the images well. However, this model together with external shear produces an excellent fit, albeit with a large shear (see column 6 in Table 3). Even a small shear such as 0.05 produces a substantially better fit than with no shear (see the last column in Table 3 and Figure 3). All the

M/L models, with or without shear, produce a minor cusp configuration. The parameter $\bar{\kappa}$ for the M/L models gives the mean κ in a circle of radius $0''.915$ about the galaxy center. If $z_L = 0.56$ and $z_S = 1.5$ then the mass within this circle is $M = 1.9 \times 10^{11} h^{-1} \bar{\kappa} M_\odot$, which yields a mass-to-light ratio of $25 h \bar{\kappa}$ for the M/L models. If we assume a small shear then $\bar{\kappa} \sim 1$ (Table 3), and the mass-to-light ratio is on the high side of the range of other lens galaxies (Keeton, Kochanek, & Falco 1998). Note, however, that we only have an estimated photometric redshift for the lens and a guess for the source redshift. The mass-to-light ratio changes to $14 h \bar{\kappa}$ for ($z_L = 0.8$, $z_S = 2.0$) and to $57 h \bar{\kappa}$ for ($z_L = 0.3$, $z_S = 1.0$).

No fourth image is detected down to the detection threshold of about 28.9 mag in F606W. This is consistent with the models, which predict a fourth image fainter by a factor of 3 or 4. The M/L models are non-singular and predict a fifth image at the lens center which would be fainter by an additional factor of ~ 100 . The best-fitting models also locate the image of the cusp near the observed position of component C, so this component can be produced if the source is extended.

4. Discussion

We have modeled a candidate gravitational lens, HDF5 2232509–603243 found in the HDF-S. The image positions can be fit in a minor cusp configuration by simple lens models which include ellipticity or shear, or with shear added to a model with a constant mass-to-light ratio. However, an exact fit is obtained only with a substantial shear produced by objects lying to the NE or SW. No obvious candidate galaxy lies within $5''$ of the lens, but if the shear is produced by a galaxy group it could be up to an arcminute away. The lensing galaxy is expected to have a redshift $z \sim 0.6$, which gives it a luminosity of roughly L^* . In the context of the gravitational lens model, the galaxy is expected to have a mass-to-light ratio of $\sim 25 h$ and a velocity dispersion of $\sim 280 \text{ km s}^{-1}$, based on the estimated photometric redshift $z = 0.56$.

Showing that the arc and the lens galaxy are at different redshifts would rule out the possibility that the arc is a tidally disrupted satellite. On 10-m-class telescopes, it is straightforward to get spectroscopic redshifts of galaxies at 22 mag, even elliptical galaxies which tend to have absorption-feature dominated spectra (Cohen et al. 1998). Some elliptical galaxies at this flux level even have measured central velocity dispersions (van Dokkum et al. 1998; Pahre 1998). Thus the prospects for follow-up spectroscopy on the elliptical are good. It is common to obtain redshifts for sources at 25 mag, even some which are close to bright nearby sources (Steidel et al. 1996), so there is hope for a spectroscopic redshift for the arc. Because it shows significant $F300W$ flux, the arc is unlikely to be at redshift $z > 2.3$. A lack of spectroscopic features in the visual will make redshift determination difficult unless the arc is at $z < 1$ (Hogg et al. 1998).

The fact that HDF5 2232509–603243 appears to be comprised of a background galaxy lensed by a field elliptical is notable given the paucity of lenses in the HDF (see §1) and the smaller number of ellipticals in the HDF-S compared to the HDF (Williams 1998).

It is a pleasure to thank Bob Williams and the entire HDF-S team for taking, reducing, and making public the beautiful images of the HDF-S. Scott Burles and Wayne Hu provided very useful help in short order. This research is based on observations made with the NASA/ESA Hubble Space Telescope, which is operated by AURA under NASA contract NAS 5-26555. Barkana and Blandford acknowledge support by Institute Funds. Hogg acknowledges Hubble Fellowship grant HF-01093.01-97A from STScI, which is operated by AURA under NASA contract NAS 5-26555.

REFERENCES

- Blandford, R. D., & Narayan, R. 1992, *ARA&A*, 30, 311
- Cohen, J. 1998, personal communication
- Cohen, J. G., Hogg, D. W., Pahre, M. A., Blandford, R., Shopbell, P. L., & Richberg, K., 1998, *ApJS* in press
- Cooray, A. R., Quashnock, J. M., & Miller, M. C. 1998, preprint astro-ph/9806080, to appear in *ApJ*
- Ellis, R. S., *Nature*, 395, A3
- Hogg, D. W., Blandford, R. D., Kundić, T., Fassnacht, C. D., & Malhotra, S. 1996, *ApJ*, 467, L73
- Hogg, D. W., Cohen, J. G., Blandford, R., & Pahre, M. A., 1998, *ApJ* 504 622
- Kassiola, A., & Kovner, I. 1993, *ApJ*, 417, 450
- Keeton, C. R., Kochanek, C. S., & Seljak, U. 1997, *ApJ*, 482, 604
- Keeton, C. R., Kochanek, C. S., & Falco, E.E. 1998, preprint astro-ph/9708161
- Kochanek, C. S. 1996, *ApJ*, 466, 638
- Kormann, R., Schneider, P., & Bartelmann, M. 1994, *A&A*, 284, 285
- Madau, P., Pozzetti, L., & Dickinson, M. 1998, *ApJ*, 498, 106
- Pahre, M. A. 1998, *ApJS* submitted
- Ratnatunga, K. U., Ostrander, E. J., Griffiths, R. E. & Im, M. 1995, *ApJ*, 453, L5
- Schneider, P., Ehlers, J., & Falco, E.E. 1992, *Gravitational Lenses* (New York: Springer)
- Steidel, C. C., Giavalisco, M., Dickinson, M. & Adelberger, K. L. 1996, *AJ*, 112, 352
- Turner, E. L., Ostriker, J. P., & Gott, J. R. 1984, *ApJ*, 284, 1

van Dokkum P. G., Franx M., Kelson D. D., & Illingworth G. D. 1998, ApJ, 504, L17

Williams, R. et al. 1996, AJ, 112, 1335

Williams, R. et al. 1998, in preparation

Williams, R. 1998, personal communication

Zepf, S. E., Moustakas, L. A., & Davis, M. 1997, ApJ, 474, L1

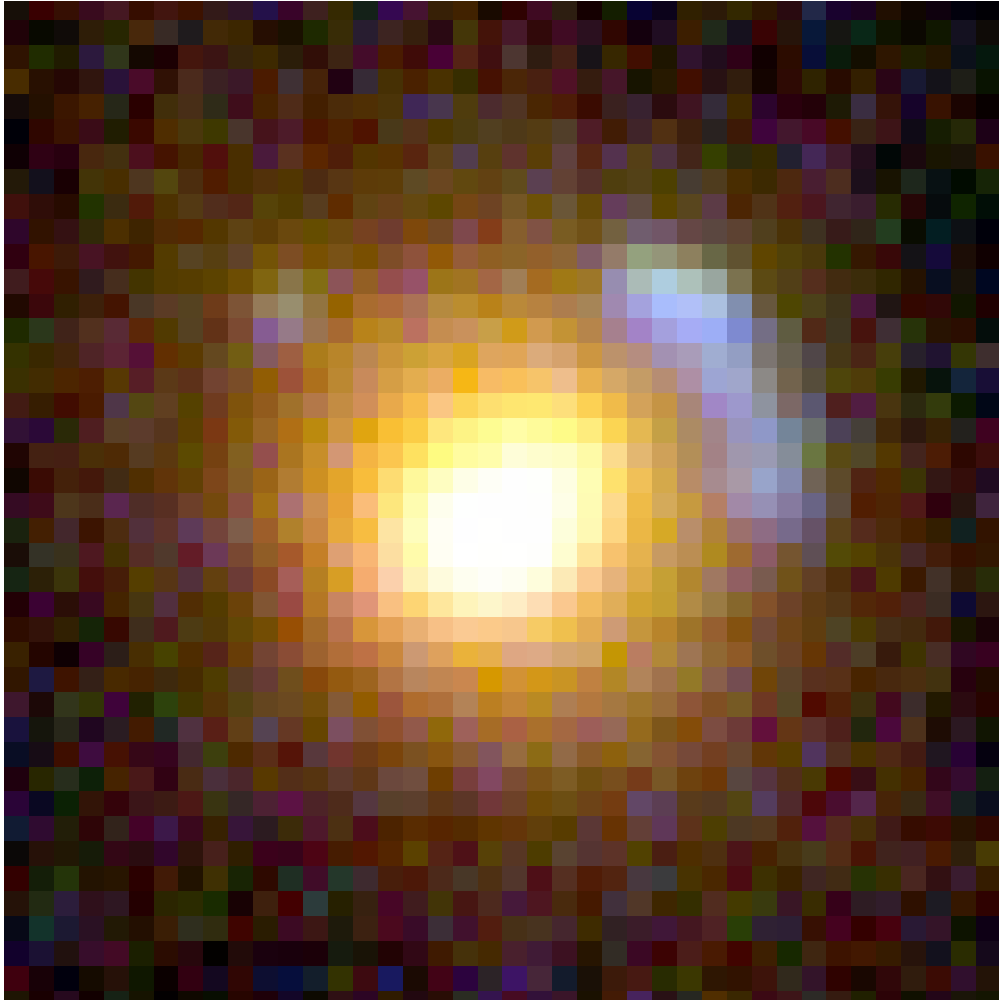


Fig. 1.— A region taken from the public release of the HDF-S (Williams et al. 1998). It shows the lens galaxy, the arc to its NW, and the dot to its NE. North is up and East is to the left (except for a 0.5° rotation). The figure is centered on the lens galaxy and measures $3''.2$ on a side.

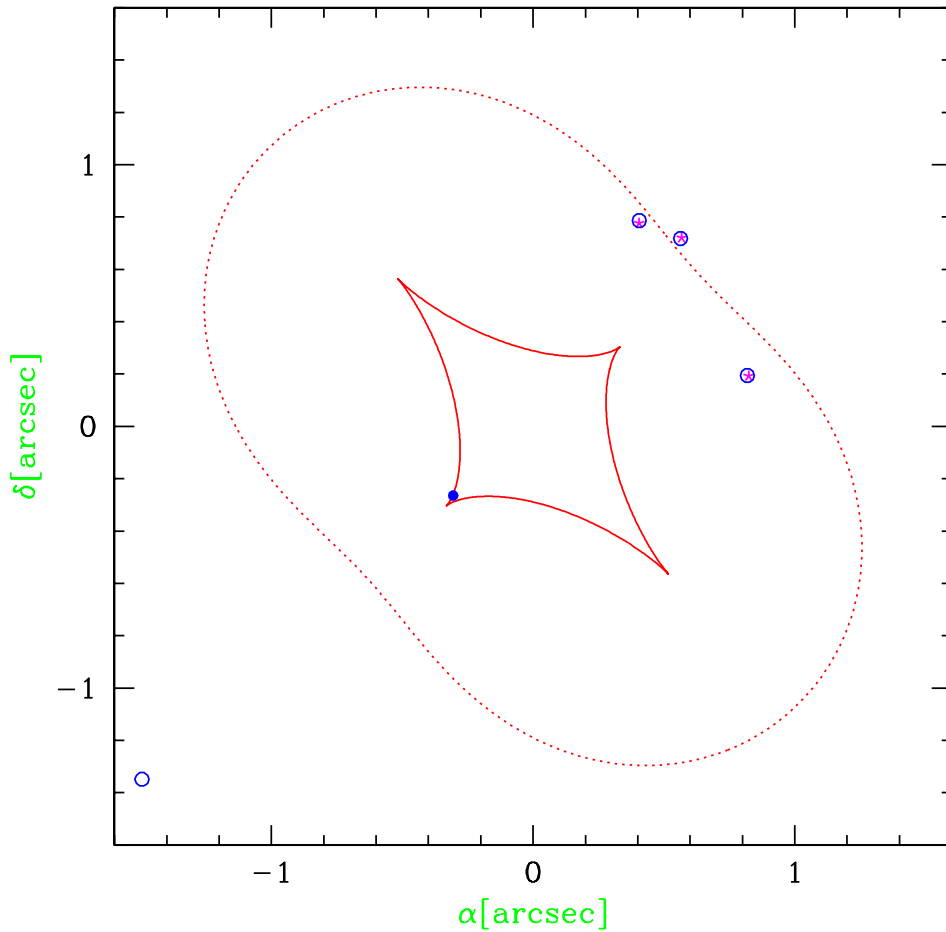


Fig. 2.— Image and source positions for the SIS+ γ [min] model (column 3 of Table 3). Four image positions (\circ) are indicated along with the source position (\bullet) and the observed positions of arc components A, B and D (\star). Also shown are the tangential caustic (solid) and critical curve (dotted). The figure is centered on the lens galaxy, with the α -direction west and the δ -direction north.

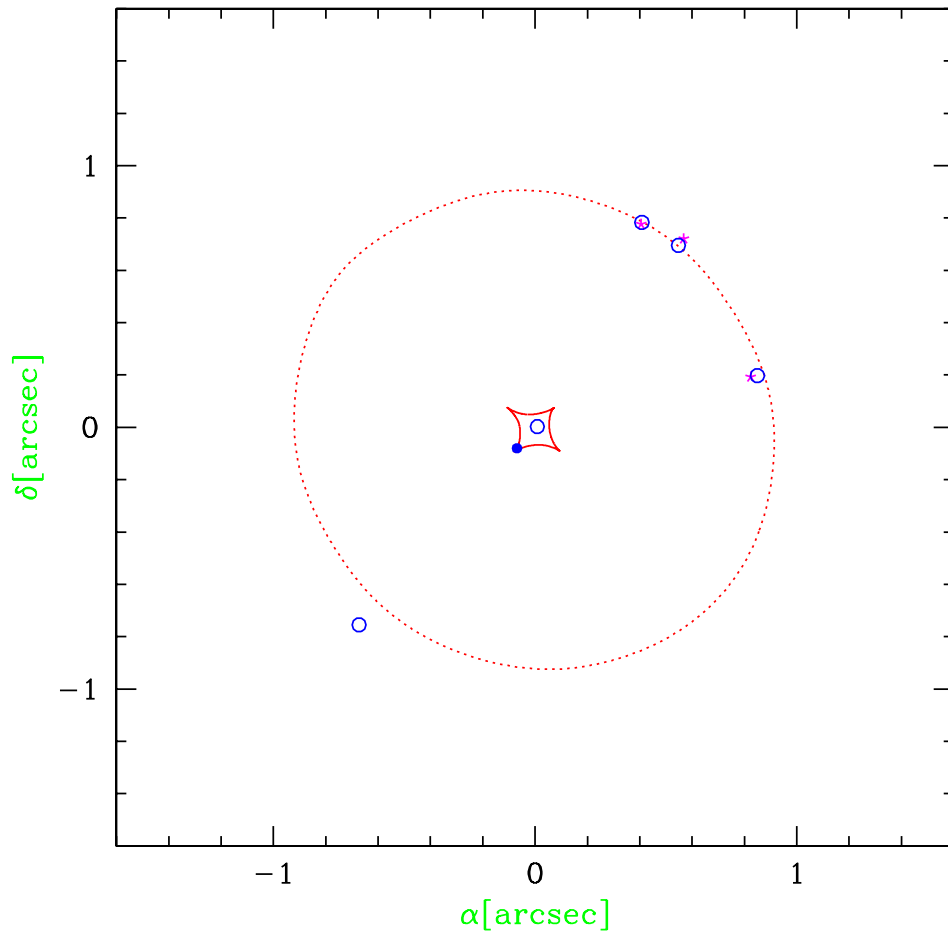


Fig. 3.— Same as Figure 2, but for the M/L+ γ model with $\gamma = 0.05$ (last column of Table 3). There are five images, although the one near the lens center is extremely faint.

Table 1. Photometry

component	flux ^a		$F300W - F450W$		$F450W - F606W$		$F606W - F814W$	
	(mag)	[snr] ^b	(mag)	[snr1,snr2] ^c	(mag)	[snr1,snr2]	(mag)	[snr1,snr2]
elliptical	$F814W = 20.52$	[950]	0.31	[9.2,99]	1.86	[99,610]	1.53	[610,1200]
arc	$F606W = 25.19$	[41]	-0.96	[11,37]	0.24	[37,51]	0.40	[51,37]
dot	$F606W = 28.70$	[6.2]	...	[-1.5,3.9]	0.39	[3.9,6.2]	-0.05	[6.2,2.9]

^aDifferent components have flux measurements in different bands and through different focal-plane apertures; see text for details.

^bSignal-to-noise ratios (snr) measure the flux through the aperture relative to the expected sky noise rms through that same aperture. See text for aperture definitions.

^cThe snr values snr1 and snr2 are for the two bandpasses involved in the color measurement, bluer first.

Table 2. Astrometry^a

sub-component	$\Delta\alpha$ (arcsec)	$\Delta\delta$ (arcsec)	$F450W$ ^b (mag)
elliptical	0	0	...
arc-A	+0.406	+0.777	27.55
arc-B	+0.568	+0.721	27.43
arc-C	+0.711	+0.478	27.08
arc-D	+0.824	+0.192	28.10
dot	-0.778	+0.567	...

^aPositions are given relative to 22 32 50.9017 -60 32 43.009 (J2000), with the α -direction west and the δ -direction north. Positional uncertainties are on the order of 0''.02.

^bThe magnitudes of the arc components are based on the fluxes of the fitted gaussians. The fluxes do not add up to the total arc flux because the magnitudes exclude some diffuse emission.

Table 3. Best fit model results

Parameter	SIEMD[min]	SIEMD[maj]	SIS+ γ [min]	SIS+ γ [maj]	M/L	M/L+ γ	M/L+ γ
b or $\bar{\kappa}$	0'85	0'84	1'08	0'87	1.10	1.40	0.998
ϵ or γ	$0.95^{+0.05}_{-0.95}$	$0.02^{+0.62}_{-0.02}$	$0.26^{+0.04}_{-0.05}$	$0.005^{+0.18}_{-0.005}$...	$0.52^{+0.15}_{-0.14}$	0.05
θ_ϵ or θ_γ	$41^\circ 2^{+2.9}_{-2.6}$	$-48^\circ 6^{+3.0}_{-3.1}$	$42^\circ 5^{+7}_{-7}$	$-49^\circ 0^{+3.5}_{-2.8}$...	$43^\circ 5^{+5}_{-5}$	$53^\circ 4$
#dof	1	1	1	1	3	1	1
$\bar{\chi}^2$	5.1	5.6	0.26	5.8	97	0.40	4.5

Note. — The best fits are formally at $\epsilon \rightarrow 1$ for the SIEMD[min] model, at $\epsilon \rightarrow 0$ for the SIEMD[maj] model, and at $\gamma \rightarrow 0$ for the SIS+ γ [maj] model. The overall best fit for the M/L+ γ model is given in column 6, while column 7 gives the best fit for this model with the restriction $\gamma = 0.05$. Where given, parameter ranges indicate 1σ uncertainties defined by $\Delta\chi^2 = \bar{\chi}^2$.